Kinetics of Intercluster Reactions between Atomically Precise Noble Metal Clusters $[Ag_{25}(DMBT)_{18}]^-$ and $[Au_{25}(PET)_{18}]^-$ in Room Temperature Solutions

Marco Neumaier,*[,‖] Ananya Baksi,[‖] Patrick Weis, Erik K. Schneider, Papri Chakraborty, Horst Hahn, Thalappil Pradeep,* and Manfred M. Kappes*

ABSTRACT: The kinetics of intercluster metal atom exchange reactions between solvated $[Ag_{25}(DMBT)_{18}]^-$ and $[Au_{25}(PET)_{18}]^-$ (DMBT and PET are 2,4-dimethylbenzenethiol and 2-phenylethanethiol, respectively, both $C_8H_{10}S$) were probed by electrospray ionization mass spectrometry and computer-based modeling. Anion mass spectra and collision induced dissociation (CID) measurements show that both cluster monomers and dimers are involved in the reactions. We have modeled the corresponding kinetics assuming a reaction mechanism in which metal atom exchange occurs through transient dimers. Our kinetic model contains three types of generic reactions: dimerization of monomers, metal atom exchange in the transient dimers, and dissociation of the dimers to monomers. There are correspondingly 377 discrete species connected by in total 1302 reactions (i.e., dimerization, dissociation and atom exchange reactions) leading to the entire series of monomeric and dimeric products $[Ag_mAu_{25-m}]^-$ (m = 1−24) and $[Ag_mAu_{50-m}]^{2-}$ (m = 0−50), respectively. The rate constants of the corresponding reactions were fitted to the experimental data, and good agreement was obtained with exchange rate constants which scale with the probability of finding a silver or gold atom in the respective monomeric subunit of the dimer, i.e., reflecting an entropic driving force for alloying. Allowing the dimerization rate constant to scale with increasing gold composition of the respective reactants improves the agreement further. The rate constants obtained are physically plausible, thus strongly supporting dimer-mediated metal atom exchange in this intercluster reaction system.

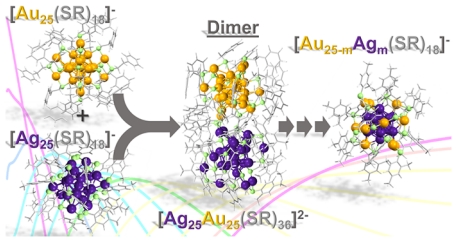

INTRODUCTION

Intercluster reactions[1−8] in homogeneous solution constitute an emerging area in the field of atomically precise nanoclusters[9−20] with great potential for the controlled formation of transition metal nanoalloys.[21−24] Reactions between different coinage metal clusters have been studied, focusing on the identification of intermediates and products via electrospray ionization mass spectrometry (ESI MS) of liquid reaction mixtures. In the first documented case, the reaction between solvated $[PPh_4^+]_4[Ag_{44}(SR)_{30}]^{4-}$ and $[TOA]^+[Au_{25}(SR)_{18}]^-$ clusters (TOA refers to tetraoctylammonium cations, SR refers to thiolate) resulted in the formation of mixed $[Ag_mAg_{25-m}(SR)_{18}]^-$($m$ = 0−20) nanoalloy clusters (i.e., having the same overall metal nuclearity).[7] In another example, reactions between solvated $Ag_{29}(BDT)_{12}(PPh_3)_4$ "superatoms" and $Cu_{12}S_6(DPPPT)_4$ clusters (BDT and DPPPT are 1,3-benzenedithiolate and bis(diphenylphosphino)pentane, respectively) have recently been shown to lead to extensive copper−silver exchange without significantly changing the structure type of the various $Ag_{29-x}Cu_x$ species formed as mixing progressed.[4] Intercluster reactions have also been reported between a coinage metal cluster and other transition metal cluster species, e.g., between $[Au_{25}(SR)_{18}]^-$ and $Ir_9(SR)_6$ clusters leading to the formation of a new bimetallic, neutral $Ir_3Au_{22}(SR)_{18}$ cluster.[5] Recently, a trimetallic dithiol protected $MAu_xAg_{28-x}(BDT)_{12}(PPh_3)_4$ (M = Ni, Pd, or Pt and x = 1−12) cluster was formed by intercluster reactions.[6]

On the basis of MS and density functional theory (DFT) calculations, Pradeep and co-workers proposed that the reaction between $[Ag_{44}(SR)_{30}]^{4-}$ and $[Au_{25}(SR)_{18}]^-$ proceeds via ligand interaction between two solvated clusters in close proximity.[7] Shortly thereafter, Bürgi et al. used a different approach to support this picture. They showed that in the "$Au_{38}(SR)_{24}$ + $Au_{38-x}Ag_x(SR)_{24}$" reaction system, separation of the two reagents by a dialysis membrane impermeable to the solvated clusters but still permeable to their smaller building blocks (<1000 Da) prevented the nanoalloying reaction completely, on the experimental time scale.[25] This implies that metal exchange via oxidative dissolution/readsorption of small component building blocks, an alternative mechanism,

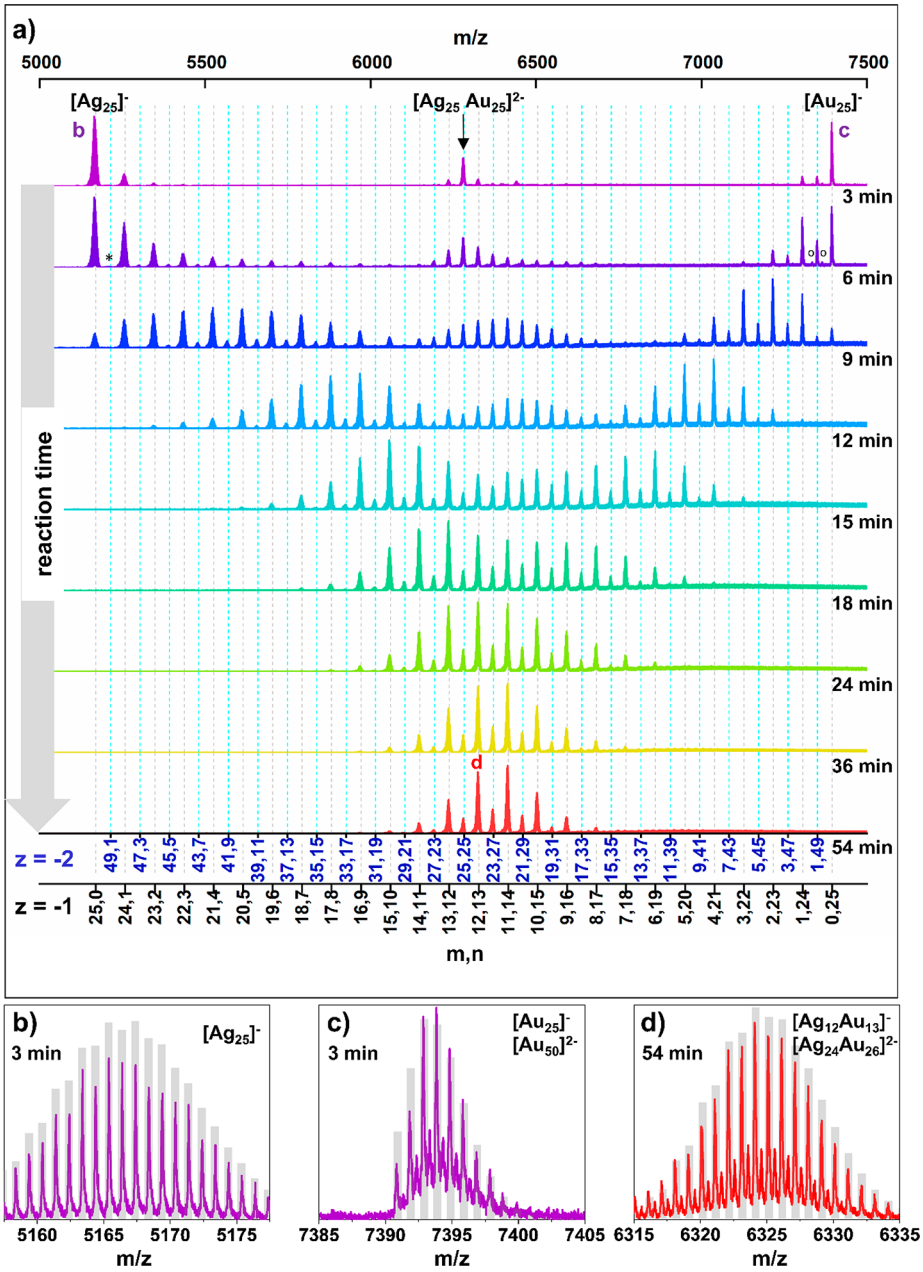

Figure 1. (a) Time dependent changes in the mass spectra of a 1:1 (40:40 nmol L ^{1}) mixture of $[Au_{25}(PET)_{18}]$ and $[Ag_{25}(DMBT)_{18}]$ over a 54 min time scale after mixing. Pairs of integers *m,n* label either $[Ag_mAu_n]$ cluster monoanions (black scale) or $[Ag_mAu_n]^2$ cluster dianions (blue scale). Gray grid lines are spaced by 89 u (the mass difference of Au and Ag) to guide the eye. The peaks on the gray grid lines correspond to both monomers $[Ag_mAu_{25\ m}]$ and the corresponding doubly charged dimers $[Ag_{2m}Au_{50\ 2m}]^2$ with even number of silver and gold atoms of the same *m/z*. Note that due to the resolved isotopic patterns, the relative intensities of both species can be deconvoluted. The cyan colored grid lines (also spaced by 89 u) correspond to doubly charged dimers with odd numbers (total) of silver and gold atoms. The peak labeled with an asterisk in the mass spectrum taken at 6 min reaction time refers to $[Ag_{49}Au]^2$. Peaks marked with a circle at 6 min correspond to triply charged trimers $[AgAu_{74}(SR)_{54}]^3$ and $[Ag_2Au_{73}(SR)_{54}]^3$. The peaks labeled with "b", "c", and "d" correspond to the clusters shown in the zoom plots b–d. (b) Isotopic distribution of $[Ag_{25}]$ after a reaction time of 3 min. Only peaks separated by 1 u are observed which shows that doubly charged $[Ag_{50}]^2$ clusters are not present. Gray bars refer to the calculated (natural) isotopic pattern of $[Ag_{25}]$. (c) (Ligand-associated) Isotopic distribution of $[Au_{25}]$ after a reaction time of 3 min. In addition to $[Au_{25}]$, $[Au_{50}]^2$ clusters are also present as indicated by additional peaks between the singly spaced $[Au_{25}]$ signals. Gray bars correspond to the calculated isotopic distribution of $[Au_{25}]$. (d) Isotopic distribution of $[Ag_{12}Au_{13}]$ after a reaction time of 54 min with underlying signal of doubly charged $[Ag_{24}Au_{26}]^2$. Gray bars refer to the calculated isotopic distribution of $[Ag_{12}Au_{13}]$.

was not kinetically competitive with the dimer mediated process.

What is the driving force for dimer-mediated nanoalloying? In a recent study, equal amounts of isotopically pure $[^{107}Ag_{25}(SR)_{18}(PPh_4)]^-$ and $[^{109}Ag_{25}(SR)_{18}(PPh_4)]^-$ were reacted in room temperature solution to form a purely statistical distribution of $[^{107}Ag_{25-x}{}^{109}Ag_x(SR)_{18}]^-$ isotopologue products.[26] Here the driving force was clearly entropic with essentially no enthalpic contributions. By contrast, enthalpic contributions might be expected to become more

important when alloying two different metals by an intercluster reaction. We recently found in the "$[Au_{25}(PET)_{18}]^-$ + $[Ag_{44}(FTP)_{30}]^{4-}$" reaction system (FTP is 4-fluorothiophenol), that although metal atom exchange starts from the outside of the M_{44} unit, i.e., in the staples, the introduced gold atoms can subsequently insert themselves into the cluster cores. Such swapping rearrangement occurs in what is presumably a thermally activated "nanogymnastic fashion" to form the most stable isomers in a matter of minutes.[27] How the initial metal exchange between two individual, negatively charged, ligand-interleaved, and staple-protected clusters starts is presently an open question. So far the picture is based only on DFT calculations of plausible intermediates.[8,28] To help clarify this further, it would be useful to provide some first order kinetic data for the three most important mechanistic steps in the overall intercluster reaction: dimer formation, metal atom exchange, and dimer dissociation. This is the motivation for the present study.

Of particular interest for the mechanistic understanding are reactions between isostructural clusters. Arguably, the simplest case concerns the eight-electron superatom[29−31] species $[Au_{25}(SR)_{18}]^-$ and $[Ag_{25}(SR)_{18}]^-$. Their reaction leads to the formation of all possible alloy clusters while always preserving 25 metal atoms and 18 ligands in the mixed monomer clusters.[28] Here we show systematic, time-resolved anion mass spectrometry measurements for the intercluster exchange reaction between $[Ag_{25}(DMBT)_{18}]^-$ and $[Au_{25}(PET)_{18}]^-$ in solution on a time scale of up to 60 min after mixing—resolving both the changing monomer compositions and concentrations and also probing those of the transiently formed dimers. Additional CID studies as a function of reaction time reveal that the fragmentation behavior of dimers qualitatively changes as the reaction proceeds and that the stability of the mixed dimers increases with mixing degree within the component monomers.

Note that specific electrospray conditions can also lead to some dimer formation in gas phase. In fact, the formation of dimers of $[Au_{25}(SR)_{18}]^-$ clusters was first studied under controlled electrospray conditions.[32] However, there are meanwhile multiple reports strongly indicating the existence of such dimers in solution and solid phase too. For example, Liu et al. reported $Ag_2Au_{50}(PET)_{36}$ dimers in solution which showed distinct optical and electronic properties, compared to those of the $Au_{25}(SR)_{18}$ clusters also present.[33] The crystal structure of this dimer was also solved. Linear polymers of $Au_{25}(SBu)_{18}$ clusters were also observed in the crystalline state.[34] Cations are known to induce dimerization of $Ag_{29}(BDT)_{12}$ clusters as well.[35] All such studies clearly indicate that the formation of dimers of clusters is not limited to selected mass spectrometric conditions but that extensive dimerization may occur spontaneously in solution or solid state as well.

In this study we have used mass spectrometry to probe dimerization induced intercluster reactions in room temperature solutions under conditions in which ion densities were too low to allow for additional dimer formation in gas phase. On the basis of the mass spectrometric data, we have modeled the kinetics of this intercluster reaction using several different mechanistic schemes which require the exchange reaction to take place *exclusively* within transiently formed dimers. The best fitting model was able to qualitatively and quantitatively describe the experimental observations. The resulting rate constants turned out to provide physically reasonable constraints on the time scales of the underlying processes.

To our knowledge this is the first quantitative kinetics study for any intercluster/nanoalloying reaction in solution. The level of agreement between best fitting simulation and experimental data extending over time scales of more than 50 min following mixing strongly supports the dimer mediated reaction hypothesis. We demonstrate that multiple, sequential dimerization and dissociation steps are involved in the chemistry, and we determine the magnitudes of the associated rate constants and from this obtain insights into the underlying atomic scale rearrangements.

RESULTS AND DISCUSSION

Mass Spectrometry and Collision Induced Dissociation. *ESI-MS.* Both $[Au_{25}(PET)_{18}]^-$ [36,37] and $[Ag_{25}(DMBT)_{18}]^-$ [38] were synthesized following previously reported methods (see the Supporting Information). The kinetics of the "$[Ag_{25}(DMBT)_{18}]^-$ + $[Au_{25}(PET)_{18}]^-$" reaction system was monitored using a high resolution Bruker timsTOF mass spectrometer system equipped with an ESI source. This ensures a typical mass resolution exceeding 25 000 which is sufficient to resolve the isotopic patterns of both singly negatively charged monomers and doubly negatively charged dimers (m/z 5000−7500; see Figure 1), which are the only metal containing species observable by ESI-MS with significant abundance. Prior to the kinetics measurements, ESI conditions were optimized such that intensities of $[Au_{25}(PET)_{18}]^-$ and $[Ag_{25}(DMBT)_{18}]^-$ were comparable for similar cluster concentrations for quantitative analyses. As dimers are more prone to fragmentation than monomers, mild electrospray conditions were chosen. The optimized measurement conditions and parameters are given in the Supporting Information (which also includes a description of the cluster synthesis and ESI mass spectra of the pure cluster solutions in Figure S1).

A typical series of averaged mass spectra of a 1:1 (40:40 nmol L^{-1}) mixture of $[Ag_{25}(DMBT)_{18}]^-$ and $[Au_{25}(PET)_{18}]^-$ taken at different reaction times is shown in Figure 1a. From previous studies it is known that in addition to metal atom exchanges, ligand exchange reactions can also occur in monothiolate-protected clusters reactions.[39−43] As the isomeric ligands DMBT and PET share the same mass and as the same number of 18 and 36 ligands is always maintained in the monomers and dimers, respectively, the DMBT-PET exchange cannot be followed by MS alone.

However, the energy changes upon ligand exchange are rather small. For the hypothetical ligand exchange reaction $[Ag_{25}(DMBT)_{18}]^-$ + $[Au_{25}(PET)_{18}]^-$ → $[Au_{25}(DMBT)_{18}]^-$ + $[Ag_{25}(PET)_{18}]^-$ we calculate (DFT, BP-86) an endothermicity of 1.26 eV, i.e., less than 0.1 eV per ligand. In similar test calculations for the single-metal exchanged clusters $[AgAu_{24}(DMBT/PET)_{18}]^-$ and $[Ag_{24}Au(DMBT/PET)_{18}]^-$ we found a negligible ligand influence on the respective isomer order (see Supporting Information for more details and Tables S1 and S2).

Therefore, in the following we will ignore the role of the ligands and from this point on we will label all species only according to the number of their silver and gold atoms. The dominant peaks visible in the spectrum after 3 min shown in Figure 1a belong to the monomers $[Ag_{25}]^-$ (m/z 5167) and $[Au_{25}]^-$ (m/z 7394) and to the dimer $[Ag_{25}Au_{25}]^{2-}$ (m/z 6280). Note that several isomers of $[Ag_{25}Au_{25}]^{2-}$ can exist in principle. For example, smaller amounts of both $[AgAu_{24}]^-$

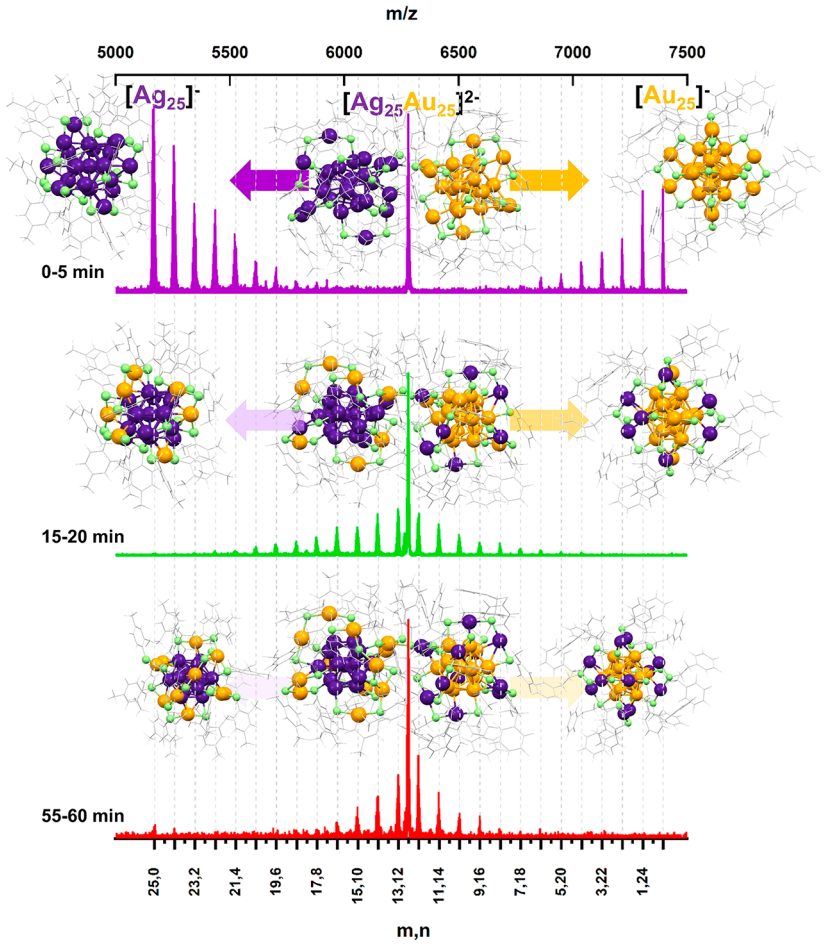

Figure 2. Collision induced dissociation of $[Au_{25}Ag_{25}]^{2}$ (m/z = 6280) clusters at 30 eV laboratory collision energy after different reaction times measured on a Waters Synapt G2Si HDMS mass spectrometer. After short reaction times of up to 5 min, the formed $[Au_{25}Ag_{25}]^{2}$ isomers dissociate primarily to $[Ag_{25}]$ and $[Au_{25}]$ as well as to a lesser degree to more mixed monomer $[Ag_mAu_{25\ m}]$ anions, e.g., $[Ag_{21}Au_4]$ and $[Ag_4Au_{21}]$. After long reaction times of up to 60 min, the main fragments are well mixed $[Ag_{13}Au_{12}]$ and $[Ag_{12}Au_{13}]$ ions pointing to a higher mixing degree of the formed $[Au_{25}Ag_{25}]^{2}$ isomers. The integrated intensity of the fragments decreases with reaction time which can be explained with a higher stability of the more mixed $[Au_{25}Ag_{25}]^{2}$ cluster isomers like $[(Ag_{12}Au_{13})(Ag_{13}Au_{12})]^{2}$. The concentration and mixing ratio of the $[Ag_{25}]$ and $[Au_{25}]$ clusters were chosen like in the kinetics experiment, i.e., 40:40 nmol L ^{1}.

and $[Ag_{24}Au]^{-}$ monomers are already present after short reaction times. Therefore, a fraction of the $[Ag_{25}Au_{25}]^{2-}$ signal is also due to $[(Ag_{24}Au)(AgAu_{24})]^{2-}$. Note that the round brackets refer to the two monomeric subunits of the corresponding doubly charged dimer.

Expanding on previous reports[1,28,32] of the initially formed dimer $[(Ag_{25})(Au_{25})]^{2-}$, we have recorded the time-dependent intensities of all dimers $[Ag_mAu_{50-m}]^{2-}$ with m = 0−49 together with those of the singly charged reaction products $[Ag_mAu_{25-m}]^{-}$ (m = 1−24), i.e., up to the fully mixed $[Ag_{13}Au_{12}]^{-}$ (m/z 6236) and $[Ag_{12}Au_{13}]^{-}$ (m/z 6325) clusters. Note that we use the notation $[Ag_mAu_{50-m}]^{2-}$ with m = 0−49 (i.e., without round brackets) to indicate all possible isomeric dimer dianions each of which comprises only monomers with 25 metal atom nuclearity. Closer inspection of the mass spectra shows that dimerization is clearly favored when gold is present in the monomers (note that dimerization is also observed in comparably concentrated pure $[Au_{25}(PET)_{18}]^{-}$ solutions (data not shown)). While $[Ag_{50}]^{2-}$ dimers are not present after 3 min (Figure 1b), $[Au_{50}]^{2-}$ dimers are clearly detected (Figure 1c) with comparable intensities to $[Ag_{25}Au_{25}]^{2-}$. In addition, the dianion $[AgAu_{49}]^{2-}$ shows a ∼15-fold higher intensity compared to $[Ag_{49}Au]^{2-}$ (peak labeled with an asterisk in Figure 1a). Dianionic species with an even number of gold and silver atoms $[Ag_{2m}Au_{50-2m}]^{2-}$ share the same m/z ratio as monoanionic species $[Ag_mAu_{25-m}]^{-}$, and their peaks overlap. Therefore, only dimers $[Ag_{2m-1}Au_{50-(2m-1)}]^{2-}$ with odd numbers of silver and gold atoms (i.e., peaks lying on the cyan colored grid lines) are directly visible in Figure 1a. We note, however, that in all cases we can clearly differentiate between monomers and dimers due to the resolved isotopic patterns (Figure 1b−d). On the gold side also less intense signals of triply charged trimers are visible, i.e., $[Ag_mAu_{75-m}(SR)_{54}]^{3-}$ with m = 1−5, which however were not further taken into account in this analysis due to their low intensity (see Figure S2).

After a longer reaction time, the dimer distribution centered around $[Ag_{25}Au_{25}]^{2-}$ broadens and other dimers such as $[Ag_{27}Au_{23}]^{2-}$ (m/z 6191) and $[Ag_{23}Au_{27}]^{2-}$(m/z 6370) appear (Figure 1a, 12 min). At the same time, more mixed monomers grow successively from the silver and gold sides of the mass spectra until an equilibrium state is reached after ∼45 min with $[Ag_{11}Au_{14}]^{-}$ and $[Ag_{12}Au_{13}]^{-}$ (Figure 1a and Figure 1d) being the dominant monomer species plus smaller contributions of monomers $[Ag_mAu_{25-m}]^{-}$ with m = 8−15 and dimers $[Ag_mAu_{50-m}]^{2-}$ with m = 18−28 (Figure 1a). The slight

Scheme 1. Illustration of the Different Reactions Considered[a]

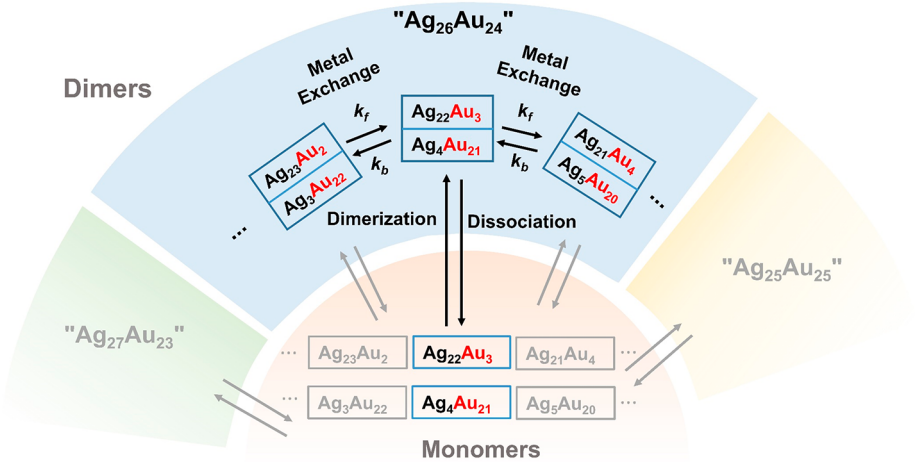

[a]Any combination of two monomers $[Ag_mAu_{25-m}]^-$ and $[Ag_nAu_{25-n}]^-$ can react to form a dimer with the sum formula $[Ag_{m+n}Au_{50-m-n}]^{2-}$ but still consisting of the well-defined monomeric subunits $[(Ag_mAu_{25-m})]^-$ and $[(Ag_nAu_{25-n})]^-$. Each dimer can isomerize via (multiple) metal atom exchanges between the monomeric subunits and separate into the respective monomers potentially at any time. Exchange rate constants k_f and k_b refer to reactions that increase (k_f) or decrease (k_b) the entropy in the dimers, respectively. As an example, we show the *m*,*n* combinations 22,3 and 4,21 for illustration. The two monomers $[Ag_{22}Au_3]^-$ and $[Ag_4Au_{21}]^-$ dimerize to form initially $[(Ag_{22}Au_3)(Ag_4Au_{21})]^{2-}$. This dimer can isomerize by metal exchange either to $[(Ag_{21}Au_4)(Ag_5Au_{20})]^{2-}$ or to $[(Ag_{23}Au_2)(Ag_3Au_{22})]^{2-}$. The isomerized dimers can undergo further metal exchange or dissociate to monomers.

asymmetry toward a higher gold content with respect to a perfect 1:1 cluster ratio where $[Ag_{12}Au_{13}]^-$ and $[Ag_{13}Au_{12}]^-$ should be the dominant species can be most likely traced back to weighing and dilution errors (the concentrations of 40 nmol L^{-1} were reached by a two-step dilution). For $[Ag_{25}]^-$:$[Au_{25}]^-$ mixing ratios differing from 1:1 the equilibrium distribution is shifted according to the silver:gold atom ratio. Hence, for a mixing ratio of $[Ag_{25}]^-$:$[Au_{25}]^-$ = 5:3 (100:60 nmol L^{-1}) the equilibrium distribution is approximately centered at around $[Ag_{16}Au_9]^-$, i.e., $\frac{5\cdot25}{3\cdot25+5\cdot25}\cdot25 \approx 16$ Ag and $\frac{3\cdot25}{3\cdot25+5\cdot25}\cdot25 \approx 9$ Au atoms (Figure S9b). As monoanion:dianion ratios (e.g., $[Ag_{12}Au_{13}]^-$:$[Ag_{24}Au_{26}]^{2-}$) stay constant after ~25 min, we conclude that from then on dimers and monomers are in dynamic equilibrium. Consequently, formation of stable dianions consisting of coalesced monomeric subunits (not able to dissociate back to monomers) can be ruled out. Otherwise, all monomers would end up in these stable dimers or in even higher oligomers, which is clearly not the case on a time scale of up to ~60 min.

Collision Induced Dissociation (CID). CID measurements were carried out using a Waters Synapt G2Si HDMS mass spectrometer equipped with an ESI source. To obtain a first order measure of reaction-time-dependent changes in the constituents of dimers with a given *m*/*z* ratio, we collided mass selected ions with nitrogen in a collision cell held at 0.02 mbar keeping the collision energy (E_{lab} = 30 eV) constant while measuring the corresponding fragment ion mass spectra. The fragments always contain 25 metal atoms indicating that the dimers consist of two weakly bound monomeric subunits with 25 metal atoms each. As an example, the CID of $[Ag_{25}Au_{25}]^{2-}$ (*m*/*z* 6280; see Figure 2) at different reaction times results in different fragmentation patterns. Initially, the dominant fragments are $[Ag_{25}]^-$, $[Au_{25}]^-$ plus smaller contributions of mixed clusters with up to about six exchanged metal atoms. After longer reaction times the fully mixed monomers $[Ag_{13}Au_{12}]^-$ and $[Au_{12}Ag_{13}]^-$ dominate. Obviously, for a given dimer composition, various isomers coexist confirming that the dimers are active participants in the reaction. The decreased fragmentation efficiency of $[Ag_{25}Au_{25}]^{2-}$ after longer reaction times points to a higher stability of late $[Ag_{25}Au_{25}]^{2-}$ species (e.g., $[(Ag_{12}Au_{13})(Ag_{13}Au_{12})]^{2-}$) compared to $[Ag_{25}Au_{25}]^{2-}$ species that are formed in the beginning of the reaction (e.g., $[(Ag_{25})(Au_{25})]^{2-}$ or $[(Ag_{24}Au)(AgAu_{24})]^{2-}$). Nevertheless, these "more mixed" dimers such as $[(Ag_{12}Au_{13})$-$(Ag_{13}Au_{12})]^{2-}$ are apparently still able to dissociate back to the respective monomers in solution (for which a dynamic dimer−monomer equilibrium is observed).

Kinetic Model. Next we fit the experimental data, which comprises reaction-time-dependent mass spectral signal intensities (assumed to be directly proportional to solution concentrations of the corresponding anionic species) for several initial $[Ag_{25}]^-$:$[Au_{25}]^-$ composition ratios. For this, we use three related kinetics models (simulations 1−3) that have common key mechanistic assumptions. Due to the complexity and the large number of reactions involved, we stress at the outset that we do not aim to simulate the experiment quantitatively. Instead, we want to compare the model with the experimental findings, narrow down the range of rate constants which still provide a reasonable description, and finally check the physical plausibility.

Key Assumptions. All simulations are based on the sequence of events shown in Scheme 1. We start with the most simple assumptions and then continuously improve the agreement with the experiment by refining the input parameters. The exchange kinetics was modeled by standard matrix algebra suites in MATLAB (see the Supporting Information, Scheme S1, and Figure S4 for more details) and by solving all kinetic differential equations numerically.

The key assumptions of our model are the following.

(1) Monomers always contain 25 metal atoms, and dimers contain 50 metal atoms reflecting the experimental findings.

(2) Two monomers $[Ag_mAu_{25-m}]^-$ and $[Ag_nAu_{25-n}]^-$ can dimerize with a bimolecular rate constant k_{dim}, and the

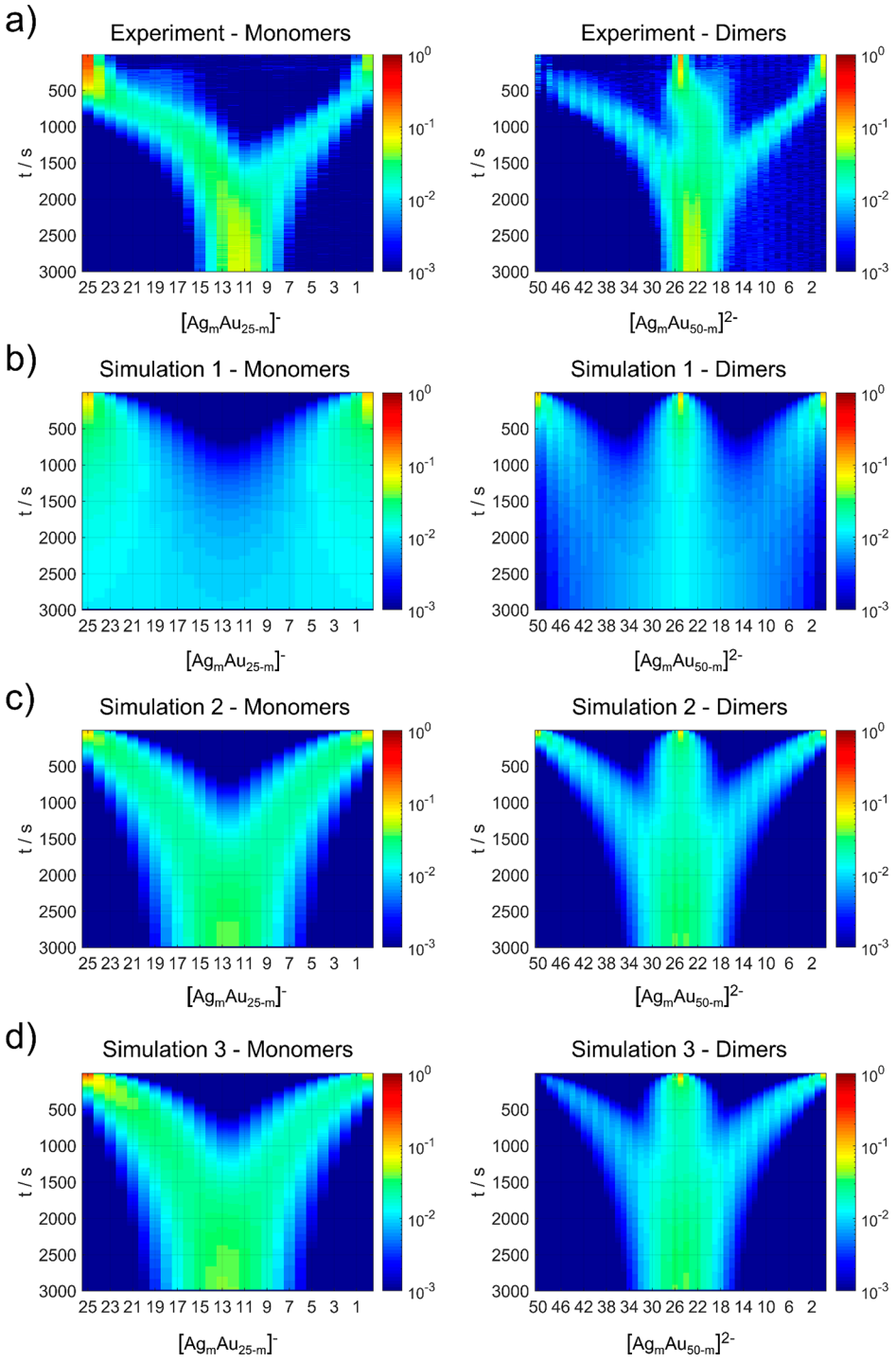

Figure 3. Contour plots of monoanionic monomer and dianionic dimer intensities for the exchange reaction between $[Ag_{25}]^-$ and $[Au_{25}]^-$. (a) Experiment (mixing ratio 40:40 nmol L^{-1}). (b) Simulation 1 (best fitting rate constants): $k_{dim} = 3.2 \times 10^{-3}$ L nmol^{-1} s^{-1}, $k_{diss} = 3.2 \times 10^{-2}$ s^{-1}, and $k_{ex} = 3.2 \times 10^{-2}$ s^{-1}. (c) Simulation 2 (best fit): $k_{dim} = 1 \times 10^{-2}$ L nmol^{-1}s^{-1}, $k_{diss} = 1 \times 10^{-1}$ s^{-1}, and $k_{ex} = 3.2 \times 10^{-2}$ s^{-1} (scaled by the probability factors from eqs 2 and 3). (d) Simulation 3 (like simulation 2 but additionally k_{dim} was scaled by the factor f_{Au}): optimum rate constants are $k_{dim} = 1 \times 10^{-2}$ L nmol^{-1}s^{-1}, $k_{diss} = 5.6 \times 10^{-2}$ s^{-1}, and $k_{ex} = 3.2 \times 10^{-2}$ s^{-1}. Starting concentrations of all simulations were chosen as in the experiment, i.e., $c([Au_{25}]^-_{t=0}) = 40$ nmol L^{-1}, $c([Au_{25}]^-_{t=0}) = 40$ nmol L^{-1} (all other species were set to concentration zero). Note that in the case of pure gold cluster solutions, dimers were already present at time zero. However, as the dimerization proceeds much faster than the metal exchange, the presence of dimers at zero time can be neglected in the simulations.

formed dimers can dissociate back with a unimolecular rate constant k_{diss}.

(3) Dimers always comprise two monomeric subunits consisting of 25 atoms which can exchange single metal atoms with a unimolecular rate constant k_{ex} (and can eventually dissociate). As a consequence, for each dimeric species with composition $[Ag_{m+n}Au_{50-m-n}]^{2-}$, there are several topologically different isomers: $[(Ag_{m-x}Au_{25-m+x})(Ag_{n+x}Au_{25-n-x})]^{2-}$ (where m and n each range from 0−25, $x \leq m$, and $x \leq (25 - n)$). We

Table 1. Summary of Simulations 1−3 As Discussed in the Text[a]

simulation	P_{ex}	f_{Au}	k_{dim}, L nmol^{-1} s^{-1}	k_{diss}, s^{-1}	k_{ex}, s^{-1}	k_{dim}:k_{diss}
1	constant	constant (=1)	3.2×10^{-3}	3.2×10^{-2}	3.2×10^{-2}	0.10
2	variable	constant (=1)	1×10^{-2}	1×10^{-1}	3.2×10^{-2}	0.10
3	variable	variable	1×10^{-2}	5.6×10^{-2}	3.2×10^{-2}	0.18

[a]The respective rate constants are obtained from a least squares fit. Overall, simulation 3 agrees best with experiment. This simulation includes an increased dimerization rate for gold rich clusters (via f_{Au}). See text for details.

allow exchange of metal atoms only within these transient dimers.

In order to compare experiment and simulation, we deconvolute the mass spectra into monomers and dimers, respectively (see the Supporting Information and Figure S3 for more details). The experimental ion intensities of monoanions and dianions for a 40:40 nmol L^{-1} mixing ratio of $[Ag_{25}]^-$ and $[Au_{25}]^-$ clusters are shown as a contour plot in Figure 3a. Each ion intensity was normalized to the total ion signal in order to account for instabilities of the ion source (see Supporting Information).

Simulation 1. In a first step we assume that the rate constants for dimerization, dissociation, and metal atom exchange are independent of the cluster composition; i.e., the kinetics is defined by only three rate constants k_{dim}, k_{diss}, and k_{ex}. Note that this is somewhat unphysical since the exchange rate constant is independent of the relative gold/silver content, but it is the most basic assumption that we can make. Simulated concentrations were treated like the experimental data (see Supporting Information) and have therefore been normalized to the sum of all ion concentrations. For all simulations a "dead time" of 20 s was chosen; i.e., at time zero in Figure 3a the reaction is assumed to have already proceeded for 20 s after mixing. Note that the choice of this "dead time" is not critical with respect to the overall kinetics as it mainly affects the time dependence of the starting species $[Ag_{25}]^-$, $[Au_{25}]^-$, and $[(Ag_{25})(Au_{25})]^{2-}$.

To find the best possible agreement between simulation and experiment, we simulated the kinetics for 13 exponentially equidistant rate constants in the range of 10^{-4} to 1 (in units of s^{-1} or L nmol^{-1} s^{-1}, respectively) resulting in 2197 ($13 \times 13 \times 13$) possible combinations.

As the dimer:monomer ratios can be affected to some degree by the mass spectrometer settings, we have chosen not the relative ion intensities but the time $t_{max,i}$ when each species i passes through its maximum concentration (as measured by ESI-MS signal) as the most robust target feature that has to be reproduced by the model. Therefore, the mean squared deviation between model and experiment was calculated with eq 1 for each simulation,

$$\chi^2 = \sum_{i=1}^{77} (t_{max,i}^{sim} - t_{max,i}^{exp})^2 \quad (1)$$

where 77 is the total number of ion species (26 monoanions: $[Ag_mAu_{25-m}]^-$, m = 0−25 and 51 dianions $[Ag_mAu_{50-m}]^{2-}$, m = 0−50). Note that in the simulation all possible 351 dimer isomers $[(Ag_{m-x}Au_{25-m+x})(Ag_{n+x}Au_{25-n-x})]^{2-}$ (m and n each range from 0−25, $x \leq m$, and $x \leq (25 - n)$) have been taken into account and summed up afterward to the corresponding $[Ag_{m+n}Au_{50-m-n}]^{2-}$ ($m + n$ = 0−50) species to allow comparison with the experiment. The number of possible dimers (351) can be determined by calculating all possible combinations of the 26 monomer species (see Supporting Information). The simulations with the lowest χ^2 values were further inspected by eye to choose the simulation with the best possible agreement in terms of both $t_{max,i}$ and relative ion intensities.

For simulation 1, a rather poor agreement was found independent of the choice of rate constants. The best possible level of agreement is shown in Figure 3b for the parameters $k_{dim} = 3.2 \times 10^{-3}$ L nmol^{-1} s^{-1}, $k_{diss} = 3.2 \times 10^{-2}$ s^{-1}, and $k_{ex} = 3.2 \times 10^{-2}$ s^{-1} (see Table 1). Compared to the experiment, the predicted cluster distributions at long reaction times are much broader and the distribution widens early. For very long reaction times (>3000 s, not shown), the monomers become evenly distributed and the dimer distribution is only determined by the number of possible isomers with a maximum of 13 for $[Ag_{25}Au_{25}]^{2-}$. The reason is the composition independent exchange rate constant k_{ex}, which leads to an even partitioning of all clusters in the equilibrium. The experimental data show that this is clearly not the case. Obviously, the model lacks a "driving force" that drags the clusters toward a narrower composition distribution.

Simulation 2. In simulation 2, we continue to keep the rate constants for the dimerization and dissociation steps constant (i.e., independent of Ag:Au composition of the respective species) but now scale the exchange rate constant according to the probability of finding a silver or gold atom in the respective monomer subunit of the dimer. We assume that all metal atoms can be exchanged independent of their position in the subunit (i.e., core, icosahedral shell, or staple atoms can be exchanged with the same probability). As an example, for a $[(Ag_{25})(Au_{25})]^{2-}$ dimer consisting of the two monoanionic subunits $[Ag_{25}]^-$ and $[Au_{25}]^-$, the probability factor for silver/gold exchange according to the scheme $[(Ag_{25})(Au_{25})]^{2-} \rightarrow [(Ag_{24}Au)(AgAu_{24})]^{2-}$ is 1. If the $[Ag_{25}Au_{25}]^{2-}$ dimer consists of the subunits $[Ag_{24}Au]^-$ and $[AgAu_{24}]^-$, the combined probability factor is $\frac{24}{25} \cdot \frac{24}{25} = 0.9216$ in the direction where the dimer becomes more mixed, $[(Ag_{24}Au)(AgAu_{24})]^{2-} \rightarrow [(Ag_{23}Au_2)(Ag_2Au_{23})]^{2-}$, and $\frac{1}{25} \cdot \frac{1}{25} = 0.0016$ in the direction $[(Ag_{24}Au)(AgAu_{24})]^{2-} \rightarrow [(Ag_{25})(Au_{25})]^{2-}$ where the dimer becomes less mixed. The remaining probability of 0.0768 corresponds to the "null" reaction where two gold or two silver atoms are swapped between the monomeric subunits. The differences in the probability factors can be interpreted as an entropic driving force that drags the cluster distribution toward a state with higher entropy, while the composition of the clusters in equilibrium is controlled by the mixing ratio of $[Ag_{25}]^-$ and $[Au_{25}]^-$, i.e., $[Ag_{13}Au_{12}]^-$ and $[Ag_{12}Au_{13}]^-$ for a 1:1 mixture. For the general case, $[(Ag_mAu_{25-m})\text{-}(Ag_nAu_{25-n})]^{2-}$ (with $m > n$), the combined probabilities for the forward and backward metal exchange reactions are given by

$$P_f^{ex} = \frac{m}{25} \cdot \frac{25 - n}{25} \quad (2)$$

$$P_b^{ex} = \frac{n}{25} \cdot \frac{25 - m}{25} \quad (3)$$

We define the forward reaction, occurring with k_f, where the silver atom is always transferred from the silver richer subunit of the dimer to the silver poorer subunit. Accordingly, the gold atom is transferred from the gold richer subunit to the gold poorer subunit. Note that by that definition the forward mixing reaction always leads to a higher total entropy in the products compared to the educts while the opposite is true for the backward reaction. As an example, for the dimer $[(Ag_{22}Au_3)(Ag_4Au_{21})]^{2-}$ the forward reaction produces $[(Ag_{21}Au_4)(Ag_5Au_{20})]^{2-}$ and the backward reaction leads to $[(Ag_{23}Au_2)(Ag_3Au_{22})]^{2-}$. For a quantitative calculation of the reaction entropy and the apparently less significant reaction energies as determined by explorative DFT calculations, see the Supporting Information.

Accordingly, in simulation 2 we scale the exchange rate constant k_{ex} by P_f^{ex} and P_b^{ex}, resulting in 600 individual rate constants for the metal atom exchange reactions.

Analogous to simulation 1, the best fitting parameter set was determined which is shown in Figure 3c for $k_{dim} = 1 \times 10^{-2}$ L nmol^{-1} s^{-1}, $k_{diss} = 1 \times 10^{-1}$ s^{-1}, and $k_{ex} = 3.2 \times 10^{-2}$ s^{-1} (see Table 1). The exchange rate constant k_{ex} has the biggest influence on the kinetic development of the clusters determining $t_{max,i}^{exp}$ while k_{dim} and k_{diss} mainly determine the intensities of monoanions and dianions. This holds true as long as k_{dim} does not become too small and rate determining. Therefore, χ^2 values of simulations with $k_{ex} = 3.2 \times 10^{-2}$ s^{-1}, k_{dim}:k_{diss} ratio of 0.1, and k_{dim} in the range of 1.8×10^{-3} to 1×10^{-1} L nmol^{-1} s^{-1} agree well within a standard deviation of 1%. In Figure S5 we contrast the experimentally observed kinetics of $[Ag_{25}Au_{25}]^{2-}$ to the integrated $[Ag_{25}Au_{25}]^{2-}$ concentration of the model. In addition, we show the normalized concentrations of all 13 $[(Ag_{25-x}Au_x)(Ag_xAu_{25-x})]^{2-}$ isomers (not individually accessible to MS) from simulation 2. The experiment and the simulation have in common that the integrated signal of $[Ag_{25}Au_{25}]^{2-}$ traverses a minimum with $[(Ag_{25})(Au_{25})]^{2-}$ being the dominant species in the beginning of the reaction and $[(Ag_{13}Au_{12})(Ag_{12}Au_{13})]^{2-}$ close to the equilibrium.

Given the few assumptions in the model, the qualitative agreement with the experiment is surprisingly good and allows the conclusion that the metal atom exchange proceeds more slowly in higher entropy dimers. Because of the statistical Bernoulli approach (eqs 2 and 3) the equilibrium distributions of the monomers and dimers of simulation 2 equal a binomial distribution. As shown in Figure S6, the experimental equilibrium distributions are somewhat narrower than the binomial distributions.

In contrast to the experimental data, the kinetics of the silver and gold sides in simulation 2 is exactly equal and symmetric. In the experiment, the monoanions generally show higher intensities on the silver side, especially at the beginning of the reaction, which can partially be explained by the better ability of gold clusters to form dimers.

Simulation 3 is based on simulation 2, but we now account for the unequal ability of the monomers to form dimers based on their composition. In contrast to $[Au_{25}]^-$, we do not observe (homo)dimers of $[Ag_{25}]^-$. It is still an open question which parameters dominate the ability to form dimers (e.g., attractive van der Waals forces between the clusters,[28,32] $\pi-\pi$ interactions[28] or metallophilic[44−46] interactions between the metal atoms in the staples[28,32] (including possibly gold dimer and/or gold nanowire formation via a "twist-and-lock" mechanism[8,34]). On the basis of recent DFT-based calculations, including relativistic semicore pseudopotentials, the dimer binding energies of $[Au_{50}]^{2-}$ and $[(Ag_{25})(Au_{25})]^{2-}$ are 2.5 and 2.1 eV, respectively, while $[Ag_{50}]^{2-}$ exhibits a significantly lower binding energy of only 0.97 eV.[8] This generally points to a better dimerization ability if gold is present in the monomers. On the other hand, the isotope exchange experiment of pure $[Ag_{25}(DMBT)_{18}]^-$ clusters[26] can only be explained by silver homo dimers as reaction intermediates. Possibly they are too weakly bound to survive the ionization process in our experiment. Recent NMR studies by Salassa et al. have shown that DMBT ligand exchange is occurring in room temperature $[Ag_{25}(DMBT)_{18}]^-$ solutions.[47] This intercluster ligand exchange can only take place through the formation of transient dimers, strongly supporting the assumption that intercluster metal exchange through transient dimers occurs in pure $[Ag_{25}(DMBT)_{18}]^-$ solutions as well.

In order to account for the asymmetry between gold and silver, in simulation 3 we loosely scale the dimerization rate constant k_{dim} by a factor f_{Au}, which accounts for the fraction of gold atoms in the reactants. As an example, for $[Ag_8Au_{17}]^-$ + $[Ag_{15}Au_{10}]^-$, f_{Au} amounts to $\frac{17+10}{50} = 0.54$. The best agreement for simulation 3 with the experiment is obtained for the rate constants $k_{dim} = 1 \times 10^{-2}$ L nmol^{-1} s^{-1}, $k_{diss} = 5.6 \times 10^{-2}$ s^{-1}, and $k_{ex} = 3.2 \times 10^{-2}$ s^{-1} (see Table 1 and Figure 3d). Other values of k_{dim} and k_{diss} give almost identical results as long the k_{dim}:k_{diss} ratio is kept at around ∼0.2. With the rate constants from simulation 2, the dimer-to-monomer ratio deviates by 40% between simulation and experiment. Simulation 3 is almost identical to simulation 2, except that (like in the experiment) the cluster distribution is now asymmetric with respect to the silver and gold sides, which is most obvious at short reaction times. In simulation 3 there are more gold rich dimers present, $[Ag_{50}]^{2-}$ is not formed, and there are less gold rich monomers present as a larger fraction of these is converted to dimers. Overall, the qualitative agreement with the experimental data has improved. Note that the choice of f_{Au} regarding the dimerization of pure $[Ag_{25}]^-$ clusters (for which f_{Au} equals zero in simulation 3) is uncritical with respect to the overall kinetics which is most obvious when comparing simulation 3 with simulation 2 ($f_{Au} = 1$ for all dimerization steps). A comparison of other measured and simulated mixing ratios based on simulation 3 showing consistently good agreement is presented in Figures S7−S9. In Figure S10 we show the composition of the modeled $[Ag_{25}Au_{25}]^{2-}$ isomers at five time intervals including the three time intervals from the CID experiment (Figure 2) and contrast the findings to the experimental CID data where $[Ag_{25}Au_{25}]^{2-}$ was brought to collision with nitrogen to further support our modeling. Note that for all simulations shown, the optimized rate constants from simulation 3 were applied.

We next discuss our findings (based on simulation 3) in more detail and try to constrain the rate constants to narrower limits.

The exchange rate constant k_{ex} has the strongest impact on the kinetic development of the intercluster reaction defining $t_{max,i}^{exp}$, whereas k_{dim} and k_{diss} mainly determine the intensities of monoanions and dianions. Hence, on the basis of our model, k_{ex} can be roughly restricted to the range 2×10^{-2} s^{-1} < k_{ex} < 5×10^{-2} s^{-1}. For a good agreement with the experimental data,

the rate constants for dimerization and dissociation can be varied to some extent, but preferably, the k_{dim}:k_{diss} ratio must lie in the range 0.1−0.3. Only then the experimentally observed equilibrium monomer-to-dimer ratio of ∼1 is reproduced.

The dimerization rate constant cannot be arbitrarily small as it then becomes rate determining and the formation of mixed clusters proceeds too slowly. For good agreement with the experiment, $k_{dim}\cdot c([M_{25}]^-)$ must be at least of the order of the exchange rate constant k_{ex}. Hence, for a cluster concentration of 40 nmol L^{-1} and $k_{ex} = 3.2 \times 10^{-2}$ s^{-1}, k_{dim} should be higher than $\sim 1 \times 10^{-3}$ L $nmol^{-1}$ s^{-1}. In contrast to this lower limit, there exists no upper limit for k_{dim} kineticswise, i.e., in terms of $t_{max,i}$. If k_{dim} is increased, the predicted dimer-to-monomer ratio increases and deviates from the experimentally observed approximately 1:1 ratio (Figure 3a). Therefore, k_{diss} has to be adjusted bearing in mind the k_{dim}:k_{diss} ratio from Table 1.

Similar considerations apply to the dissociation rate constant k_{diss}. If k_{diss} is too small, early dimers like $[(Ag_{25})(Au_{25})]^{2-}$ or $[Au_{50}]^{2-}$ are almost frozen out and monomeric product ions are formed insufficiently and on time scales that are not in line with the experimental findings. Hence, within our model, k_{diss} must be greater than or equal to $\sim 1 \times 10^{-2}$ s^{-1}. Similar to the case of k_{dim}, an upper limit for k_{diss} cannot really be given (as it also depends on k_{dim}).

Plausibility of Rate Constant Values. The physical upper limit for the dimerization rate constant of near-spherical, neutral molecules in solution is the diffusion limited case for which the rate constant is given by

$$k_D = \frac{8}{3}\frac{k_B T}{\eta} N_A \tag{4}$$

where k_B is the Boltzmann constant, T is the temperature, N_A is the Avogadro constant, and η is the dynamic viscosity of the solvent (DMF).[48] With $\eta = 0.799 \times 10^{-3}$ Pa·s [49] and $T = 298$ K, k_D amounts to 8.3 L $nmol^{-1}$ s^{-1}, which is approximately 3 orders of magnitude larger than typical dimerization rate constants from our simulations. In the case of charged molecules the diffusion limited rate constant of eq 4 must be multiplied by the Debye factor f_{Debye} which accounts for the Coulomb interaction between the ions.[50−52]

$$f_{Debye} = \frac{q_A q_B}{4\pi\varepsilon_0\varepsilon_r R k_B T}\left[\exp\left(\frac{q_A q_B}{4\pi\varepsilon_0\varepsilon_r R k_B T}\right) - 1\right]^{-1} \tag{5}$$

Here q_A and q_B are the charges of the ions, ε_0 is the vacuum permittivity, ε_r is the relative permittivity of the solvent (DMF, $\varepsilon_r = 38.4$),[53] and R is the reaction distance which we assume to be twice the radius of the $[Au_{25}]^-$ cluster ($r = 6.35$ Å).[37] As shown in Figure S11, f_{Debye} equals 0.53 at a distance of 12.7 Å and the diffusion limited rate constant reduces to 4.4 L $nmol^{-1}$ s^{-1} which is still a factor of ∼500 higher than the deduced dimerization rate constant estimated from our model (a deviation that we rationalize as due to finite activation energies for dimerization).

There is very little experimental data on the dimerization of other solvated, equicharged, aryl-terminated clusters in the 1 nm size range to compare with. Biopolymer anions whose dimerization may also involve $\pi-\pi$ interactions are better studied in this regard. For example, oligoribonucleotides with a chain length between four and seven nucleotides combine with a bimolecular rate constant of 2×10^{-3} L $nmol^{-1}$ s^{-1}, and typical dissociation rates of double stranded dye-labeled oligomers consisting of 10 base pairs were determined to $\sim 1 \times 10^{-2}$ s^{-1}.[54,55] The (dimer) dissociation rate decreases strongly with increasing oligomer size at a given temperature.[54] Gotoh et al. found a dissociation rate constant of 1.2×10^{-4} s^{-1} for a 20-mer oligonucleotide.[56] Our determined rate constants for dimerization and dimer dissociation are in surprisingly good agreement with these numbers, despite the different systems, concentrations, and solvents (perhaps fortuitously).

According to eq 6, k_{diss} directly determines the average lifetime τ of the cluster dimers for which we may estimate an upper limit of ∼100 s.

$$\tau = \frac{1}{k_{diss}} \tag{6}$$

The number of exchange reactions during the lifetime τ of the dimer dianion can be estimated by Poisson statistics,

$$P(k) = \frac{(k_{ex}\tau)^k \, e^{-(k_{ex}\tau)}}{k!} \tag{7}$$

where $P(k)$ is the probability of k exchange reactions to occur during the lifetime τ of the dimer and k_{ex} is the exchange rate constant. With $\tau = 0.056^{-1}$ s ≈ 18 s, on average 0.5 exchanges occur in the dimers, and with the upper limit $\tau = 0.01^{-1}$ s = 100 s, on average 3.2 exchanges occur.

Although the overall agreement between the simulations and experiment is good in terms of kinetics, the observed experimental equilibrium distributions are somewhat narrower compared to the corresponding binomial distributions from the simulation. Similar observations have been made by Zhang et al. when doping silver atoms into $Au_{38}(SC_2H_4Ph)_{24}$ clusters.[25] It was found that a cluster distribution centered around $Ag_{6.5}Au_{38-6.5}$ became significantly sharper over a time scale of 3 h. The authors argued that not all possible 38 positions in the cluster are occupied by silver atoms with the same probability. On the basis of our own DFT calculations (see the Supporting Information) and on the basis of findings by Krishnadas et al.,[28] the staple and icosahedral center positions in a $M_{25}(SR_{18})$ cluster are preferentially occupied by gold atoms while the 12 icosahedron core positions are preferentially occupied by silver atoms. These results are largely in line with the X-ray structure analysis of $Au_{18.8}Ag_{6.2}(SCH_2CH_2Ph)_{18}$ where approximately equal partitioning of silver and gold in the icosahedral core was found, while gold atoms clearly favored the staple and the icosahedron central position.[57]

In a recent study it was proposed on the basis of DFT calculations that the metal atom exchange in the "$[Au_{25}(PET)_{18}]^-$ + $[Ag_{25}(DMBT)_{18}]^-$" system takes place in a two-step fashion where first exchange of staple metal atoms takes place followed by swapping of heterometal atoms into the icosahedral M_{13}-kernel.[8] Conceivably, such stabilizing intracluster rearrangement processes occur on a time scale that is (significantly) longer than that of metal exchange as inferred here. This could explain why the kinetics and (near) equilibrium composition distributions observed on time scales of >30 min appear mainly entropically driven but are narrower than binomial distributions in detail.

Note that if no intracluster rearrangement took place at all, only the staple atoms could participate in metal atom exchange, i.e., only 48% ($=\frac{12}{25}\cdot 100\%$) of the silver atoms of

Ag_{25}^- would be available for the doping of the Au_{25}^- cluster. Hence, for a mixing ratio of Ag_{25}:Au_{25} of 3:5, the cluster equilibrium distribution would be centered around $Ag_{4.5}Au_{20.5}^-$ ($\frac{3\cdot12}{3\cdot25+5\cdot25}\cdot25 \approx 4.5$) and not around $Ag_9Au_{16}^-$ as observed in the experiment. This simple consideration clearly shows that also metal atoms in the icosahedral shell (and center) must participate in the reaction over the 60 min time scale probed.

CONCLUSIONS

We have explored the kinetics of intercluster metal exchange reactions between $[Ag_{25}(DMBT)_{18}]^-$ and $[Au_{25}(PET)_{18}]^-$ in room temperature solutions by probing the solution composition with high resolution electrospray ionization mass spectrometry over a time scale of 60 min from the beginning of the reaction. For the cluster concentrations probed (40−100 nmol L^{-1}), anion mass spectra show significant amounts of both cluster monomers and dimers, with changing overall Ag:Au compositions that track synchronously with reaction time before finally approaching a dynamic equilibrium. We have modeled the corresponding kinetics assuming that the mass spectra essentially reflect the solution composition. Consistent with previous literature on related intercluster reactions, we have assumed a reaction mechanism in which metal atom exchange can only occur during transient dimer formation. Specifically, our simple kinetic model contains three generic reactions: dimerization of monomers, metal atom exchange in the transient dimer, and dimer dissociation. In detail, there are multiple isomeric forms to consider. If one takes this accurately into account, there are potentially 377 species involved and 1302 reactions occurring for which the rate constants are unknown a priori. We have therefore attempted to constrain the range of possible rate constants by comparing the predictions of our kinetic model with experiment under a number of further simplifying assumptions (simulations 1−3). Best agreement with measurements for several different starting composition ratios was obtained by simulation 3, where

(i) metal atom exchange rates were allowed to scale with the probability of finding a silver or gold atom in the respective subunit of the dimer, where this is equivalent to an entropic driving force (by way of assuming all possible substitutional isomers in the 50 atom dimers contribute equally to the exchange process), and
(ii) the dimerization rate constants were allowed to scale with increasing gold composition of the respective educts.

The rate constants then obtained are physically plausible also when compared to measurements of the dimerization and dimer dissociation rates of oligoribonucleotides. Like the aryl-ligand interleaved transient dimer formation invoked here, these solution reactions also involve association/dissociation of two negatively charged educts. Altogether, our kinetic study strongly supports dimer mediated metal atom exchange in this intercluster reaction system. It points to future research using structure sensitive gas-phase methods such as energy resolved CID, high resolution ion mobility spectrometry, or trapped ion electron diffraction to explore a range of remaining issues, e.g., (i) What is the detailed reaction path leading to a transient dimer configuration able to exchange metal atoms? (ii) How does this depend on the type of terminating ligands? (iii) To what extent are the ligands then involved in mediating the actual metal atom exchange? (iv) Once the exchange has occurred, what is the kinetics of site-specific metal atom interdiffusion processes between staple, icosahedral core and center positions?

AUTHOR INFORMATION

Corresponding Authors

Marco Neumaier − *Institute of Nanotechnology, Karlsruhe Institute of Technology, 76344 Eggenstein-Leopoldshafen, Germany;* orcid.org/0000-0002-3810-3377; Email: marco.neumaier@kit.edu

Thalappil Pradeep − *DST Unit of Nanoscience and Thematic Unit of Excellence, Indian Institute of Technology Madras, 600 036 Chennai, India;* orcid.org/0000-0003-3174-534X; Email: pradeep@iitm.ac.in

Manfred M. Kappes − *Institute of Nanotechnology, Karlsruhe Institute of Technology, 76344 Eggenstein-Leopoldshafen, Germany; Institute of Physical Chemistry, Karlsruhe Institute of Technology, 76131 Karlsruhe, Germany;* orcid.org/0000-0002-1199-1730; Email: manfred.kappes@kit.edu

Authors

Ananya Baksi − *Institute of Nanotechnology, Karlsruhe Institute of Technology, 76344 Eggenstein-Leopoldshafen, Germany;* orcid.org/0000-0003-3328-4399

Patrick Weis − *Institute of Physical Chemistry, Karlsruhe Institute of Technology, 76131 Karlsruhe, Germany;* orcid.org/0000-0001-7006-6759

Erik K. Schneider − *Institute of Physical Chemistry, Karlsruhe Institute of Technology, 76131 Karlsruhe, Germany*

Papri Chakraborty − *Institute of Nanotechnology, Karlsruhe Institute of Technology, 76344 Eggenstein-Leopoldshafen, Germany; Institute of Physical Chemistry, Karlsruhe Institute of Technology, 76131 Karlsruhe, Germany*

Horst Hahn − *Institute of Nanotechnology, Karlsruhe Institute of Technology, 76344 Eggenstein-Leopoldshafen, Germany;* orcid.org/0000-0001-9901-3861

Author Contributions

‖M.N. and A.B. have contributed equally.

Notes

The authors declare no competing financial interest.

ACKNOWLEDGMENTS

M.M.K., H.H., and T.P. thank DFG/DST for support of an Indo-German collaborative project (Grants KA 972/11-1, HA 1344/47-1, and DST/INT/FRG/DFG/P-01/2020). M.M.K. thanks KIT for funding of the timsTOFMS used in this study. P.W. and M.M.K. thank the DFG funded collaborative research center "3MET" (TRR 88, Subproject C6) for funding which led to development of data analysis methods also used in

this project. T.P. acknowledges funding for the Centre of Excellence on Molecular Materials and Functions under the Institution of Eminence scheme of IIT Madras.

REFERENCES

(1) Krishnadas, K. R.; Baksi, A.; Ghosh, A.; Natarajan, G.; Som, A.; Pradeep, T. Interparticle Reactions: An Emerging Direction in Nanomaterials Chemistry. *Acc. Chem. Res.* **2017**, *50*, 1988−1996.

(2) Chakraborty, I.; Pradeep, T. Atomically Precise Clusters of Noble Metals: Emerging Link between Atoms and Nanoparticles. *Chem. Rev.* **2017**, *117*, 8208−8271.

(3) Krishnadas, K. R.; Baksi, A.; Ghosh, A.; Natarajan, G.; Pradeep, T. Manifestation of Geometric and Electronic Shell Structures of Metal Clusters in Intercluster Reactions. *ACS Nano* **2017**, *11*, 6015−6023.

(4) Baksi, A.; Schneider, E. K.; Weis, P.; Chakraborty, I.; Fuhr, O.; Lebedkin, S.; Parak, W. J.; Kappes, M. M. Linear Size Contraction of Ligand Protected Ag_{29} Clusters by Substituting Ag with Cu. *ACS Nano* **2020**, *14*, 15064−15070.

(5) Bhat, S.; Baksi, A.; Mudedla, S. K.; Natarajan, G.; Subramanian, V.; Pradeep, T. $Au_{22}Ir_3(PET)_{18}$: An Unusual Alloy Cluster through Intercluster Reaction. *J. Phys. Chem. Lett.* **2017**, *8*, 2787−2793.

(6) Khatun, E.; Chakraborty, P.; Jacob, B. R.; Paramasivam, G.; Bodiuzzaman, M.; Dar, W. A.; Pradeep, T. Intercluster Reactions Resulting in Silver-Rich Trimetallic Nanoclusters. *Chem. Mater.* **2020**, *32*, 611−619.

(7) Krishnadas, K. R.; Ghosh, A.; Baksi, A.; Chakraborty, I.; Natarajan, G.; Pradeep, T. Intercluster Reactions between $Au_{25}(SR)_{18}$ and $Ag_{44}(SR)_{30}$. *J. Am. Chem. Soc.* **2016**, *138*, 140−148.

(8) Huang, B.; Pei, Y. On the Mechanism of Inter-Cluster Alloying Reactions: Two-Stage Metal Exchange of $[Au_{25}(PET)_{18}]$ and $[Ag_{25}(DMBT)_{18}]$ Clusters. *J. Mater. Chem. A* **2020**, *8*, 10242−10251.

(9) Yang, J.; Jin, R. New Advances in Atomically Precise Silver Nanoclusters. *ACS Mater. Lett.* **2019**, *1*, 482−489.

(10) Kurashige, W.; Niihori, Y.; Sharma, S.; Negishi, Y. Precise Synthesis, Functionalization and Application of Thiolate-Protected Gold Clusters. *Coord. Chem. Rev.* **2016**, *320−321*, 238−250.

(11) Jin, R.; Zeng, C.; Zhou, M.; Chen, Y. Atomically Precise Colloidal Metal Nanoclusters and Nanoparticles: Fundamentals and Opportunities. *Chem. Rev.* **2016**, *116*, 10346−10413.

(12) Maity, P.; Xie, S.; Yamauchi, M.; Tsukuda, T. Stabilized Gold Clusters: From Isolation toward Controlled Synthesis. *Nanoscale* **2012**, *4*, 4027.

(13) Yao, Q.; Wu, Z.; Liu, Z.; Lin, Y.; Yuan, X.; Xie, J. Molecular Reactivity of Thiolate-Protected Noble Metal Nanoclusters: Synthesis, Self-Assembly, and Applications. *Chem. Sci.* **2021**, *12*, 99−127.

(14) Aikens, C. M. Electronic and Geometric Structure, Optical Properties, and Excited State Behavior in Atomically Precise Thiolate-Stabilized Noble Metal Nanoclusters. *Acc. Chem. Res.* **2018**, *51*, 3065−3073.

(15) Häkkinen, H. Atomic and Electronic Structure of Gold Clusters: Understanding Flakes, Cages and Superatoms from Simple Concepts. *Chem. Soc. Rev.* **2008**, *37*, 1847.

(16) Comby-Zerbino, C.; Bertorelle, F.; Dugourd, P.; Antoine, R.; Chirot, F. Structure and Charge Heterogeneity in Isomeric $Au_{25}(MBA)_{18}$ Nanoclusters -Insights from Ion Mobility and Mass Spectrometry. *J. Phys. Chem. A* **2020**, *124*, 5840−5848.

(17) Price, R. C.; Whetten, R. L. All-Aromatic, Nanometer-Scale, Gold-Cluster Thiolate Complexes. *J. Am. Chem. Soc.* **2005**, *127*, 13750−13751.

(18) Alhilaly, M. J.; Huang, R. W.; Naphade, R.; Alamer, B.; Hedhili, M. N.; Emwas, A. H.; Maity, P.; Yin, J.; Shkurenko, A.; Mohammed, O. F.; Eddaoudi, M.; Bakr, O. M. Assembly of Atomically Precise Silver Nanoclusters into Nanocluster-Based Frameworks. *J. Am. Chem. Soc.* **2019**, *141*, 9585−9592.

(19) Pollitt, S.; Truttmann, V.; Haunold, T.; Garcia, C.; Olszewski, W.; Llorca, J.; Barrabés, N.; Rupprechter, G. The Dynamic Structure of $Au_{38}(SR)_{24}$ Nanoclusters Supported on CeO_2 upon Pretreatment and CO Oxidation. *ACS Catal.* **2020**, *10*, 6144−6148.

(20) Wang, S.; Song, Y.; Jin, S.; Liu, X.; Zhang, J.; Pei, Y.; Meng, X.; Chen, M.; Li, P.; Zhu, M. Metal Exchange Method Using Au_{25} Nanoclusters as Templates for Alloy Nanoclusters with Atomic Precision. *J. Am. Chem. Soc.* **2015**, *137*, 4018−4021.

(21) Ferrando, R.; Jellinek, J.; Johnston, R. L. Nanoalloys: From Theory to Applications of Alloy Clusters and Nanoparticles. *Chem. Rev.* **2008**, *108*, 845−910.

(22) Calvo, F. Thermodynamics of Nanoalloys. *Phys. Chem. Chem. Phys.* **2015**, *17*, 27922−27939.

(23) Peng, L.; Ringe, E.; Van Duyne, R. P.; Marks, L. D. Segregation in Bimetallic Nanoparticles. *Phys. Chem. Chem. Phys.* **2015**, *17*, 27940−27951.

(24) Ferrando, R. Symmetry Breaking and Morphological Instabilities in Core-Shell Metallic Nanoparticles. *J. Phys.: Condens. Matter* **2015**, *27*, 013003.

(25) Zhang, B.; Salassa, G.; Bürgi, T. Silver Migration between $Au_{38}(SC_2H_4Ph)_{24}$ and Doped $Ag_xAu_{38-x}(SC_2H_4Ph)_{24}$ Nanoclusters. *Chem. Commun.* **2016**, *52*, 9205−9207.

(26) Chakraborty, P.; Nag, A.; Natarajan, G.; Bandyopadhyay, N.; Paramasivam, G.; Panwar, M. K.; Chakrabarti, J.; Pradeep, T. Rapid Isotopic Exchange in Nanoparticles. *Sci. Adv.* **2019**, *5*, eaau7555.

(27) Baksi, A.; Schneider, E. K.; Weis, P.; Krishnadas, K. R.; Ghosh, D.; Hahn, H.; Pradeep, T.; Kappes, M. M. Nanogymnastics: Visualization of Intercluster Reactions by High-Resolution Trapped Ion Mobility Mass Spectrometry. *J. Phys. Chem. C* **2019**, *123*, 28477−28485.

(28) Krishnadas, K. R.; Baksi, A.; Ghosh, A.; Natarajan, G.; Pradeep, T. Structure-Conserving Spontaneous Transformations between Nanoparticles. *Nat. Commun.* **2016**, *7*, 13447.

(29) Kappes, M. M.; Kunz, R. W.; Schumacher, E. Production of Large Sodium Clusters (Na_x, $x \leq 65$) by Seeded Beam Expansions. *Chem. Phys. Lett.* **1982**, *91*, 413−418.

(30) Knight, W. D.; Clemenger, K.; De Heer, W. A.; Saunders, W. A.; Chou, M. Y.; Cohen, M. L. Electronic Shell Structure and Abundances of Sodium Clusters. *Phys. Rev. Lett.* **1984**, *52*, 2141−2143.

(31) Walter, M.; Akola, J.; Lopez-Acevedo, O.; Jadzinsky, P. D.; Calero, G.; Ackerson, C. J.; Whetten, R. L.; Gronbeck, H.; Hakkinen, H. A Unified View of Ligand-Protected Gold Clusters as Superatom Complexes. *Proc. Natl. Acad. Sci. U. S. A.* **2008**, *105*, 9157−9162.

(32) Baksi, A.; Chakraborty, P.; Bhat, S.; Natarajan, G.; Pradeep, T. $[Au_{25}(SR)_{18}]_2^{2-}$: A Noble Metal Cluster Dimer in the Gas Phase. *Chem. Commun.* **2016**, *52*, 8397−8400.

(33) Liu, X.; Saranya, G.; Huang, X.; Cheng, X.; Wang, R.; Chen, M.; Zhang, C.; Li, T.; Zhu, Y. $Ag_2Au_{50}(PET)_{36}$ Nanocluster: Dimeric Assembly of $Au_{25}(PET)_{18}$ Enabled by Silver Atoms. *Angew. Chem., Int. Ed.* **2020**, *59*, 13941−13946.

(34) De Nardi, M.; Antonello, S.; Jiang, D. E.; Pan, F.; Rissanen, K.; Ruzzi, M.; Venzo, A.; Zoleo, A.; Maran, F. Gold Nanowired: A Linear $(Au_{25})_n$ Polymer from Au_{25} Molecular Clusters. *ACS Nano* **2014**, *8*, 8505−8512.

(35) Chakraborty, P.; Baksi, A.; Mudedla, S. K.; Nag, A.; Paramasivam, G.; Subramanian, V.; Pradeep, T. Understanding Proton Capture and Cation-Induced Dimerization of $[Ag_{29}(BDT)_{12}]^{3-}$ Clusters by Ion Mobility Mass Spectrometry. *Phys. Chem. Chem. Phys.* **2018**, *20*, 7593−7603.

(36) Heaven, M. W.; Dass, A.; White, P. S.; Holt, K. M.; Murray, R. W. Crystal Structure of the Gold Nanoparticle $[N(C_8H_{17})_4]$-$[Au_{25}(SCH_2CH_2Ph)_{18}]$. *J. Am. Chem. Soc.* **2008**, *130*, 3754−3755.

(37) Zhu, M.; Aikens, C. M.; Hollander, F. J.; Schatz, G. C.; Jin, R. Correlating the Crystal Structure of A Thiol-Protected Au_{25} Cluster and Optical Properties. *J. Am. Chem. Soc.* **2008**, *130*, 5883−5885.

(38) Joshi, C. P.; Bootharaju, M. S.; Alhilaly, M. J.; Bakr, O. M. $[Ag_{25}(SR)_{18}]$: The "Golden" Silver Nanoparticle. *J. Am. Chem. Soc.* **2015**, *137*, 11578−11581.

(39) Niihori, Y.; Kikuchi, Y.; Kato, A.; Matsuzaki, M.; Negishi, Y. Understanding Ligand-Exchange Reactions on Thiolate-Protected

Gold Clusters by Probing Isomer Distributions Using Reversed-Phase High-Performance Liquid Chromatography. *ACS Nano* **2015**, *9*, 9347−9356.
(40) Caragheorgheopol, A.; Chechik, V. Mechanistic Aspects of Ligand Exchange in Au Nanoparticles. *Phys. Chem. Chem. Phys.* **2008**, *10*, 5029−5041.
(41) Niihori, Y.; Kurashige, W.; Matsuzaki, M.; Negishi, Y. Remarkable Enhancement in Ligand-Exchange Reactivity of Thiolate-Protected Au_{25} Nanoclusters by Single Pd Atom Doping. *Nanoscale* **2013**, *5*, 508−512.
(42) Shibu, E. S.; Muhammed, M. A. H.; Tsukuda, T.; Pradeep, T. Ligand Exchange of $Au_{25}SG_{18}$ Leading to Functionalized Gold Clusters: Spectroscopy, Kinetics, and Luminescence. *J. Phys. Chem. C* **2008**, *112*, 12168−12176.
(43) Baghdasaryan, A.; Martin, K.; Lawson Daku, L. M.; Mastropasqua Talamo, M.; Avarvari, N.; Bürgi, T. Ligand Exchange Reactions on the Chiral Au_{38} Cluster: CD Modulation Caused by the Modification of the Ligand Shell Composition. *Nanoscale* **2020**, *12*, 18160−18170.
(44) Schmidbaur, H. The Aurophilicity Phenomenon: A Decade of Experimental Findings, Theoretical Concepts and Emerging Applications. *Gold Bull.* **2000**, *33*, 3−10.
(45) Schmidbaur, H.; Schier, A. Aurophilic Interactions as a Subject of Current Research: An up-Date. *Chem. Soc. Rev.* **2012**, *41*, 370−412.
(46) Schmidbaur, H.; Schier, A. Argentophilic Interactions. *Angew. Chem., Int. Ed.* **2015**, *54*, 746−784.
(47) Salassa, G.; Krishnadas, K. R.; Pupier, M.; Viger-Gravel, J.; Bürgi, T. Role of Intercluster and Interligand Dynamics of $[Ag_{25}(DMBT)_{18}]$ Nanoclusters by Multinuclear Magnetic Resonance Spectroscopy. *J. Phys. Chem. C* **2021**, *125*, 2524−2530.
(48) Hasinoff, B. B. Simultaneous Diffusion and Chemical Activation Control of the Kinetics of the Binding of Carbon Monoxide to Ferroprotoporphyrin IX in Glycerol-Water Mixtures of High Viscosity. *Can. J. Chem.* **1977**, *55*, 3955−3960.
(49) Han, K. J.; Oh, J. H.; Park, S. J.; Gmehling, J. Excess Molar Volumes and Viscosity Deviations for the Ternary System N,N-Dimethylformamide + N-Methylformamide + Water and the Binary Subsystems at 298.15 K. *J. Chem. Eng. Data* **2005**, *50*, 1951−1955.
(50) Takahashi, K.; Bartels, D. M.; Cline, J. A.; Jonah, C. D. Reaction Rates of the Hydrated Electron with NO_2^-, NO_3^-, and Hydronium Ions as a Function of Temperature from 125 to 380 °C. *Chem. Phys. Lett.* **2002**, *357*, 358−364.
(51) Hemmes, P. On the Possibility of Like-Charged Ion Pairing in Solution. *J. Am. Chem. Soc.* **1972**, *94*, 75−76.
(52) Rice, S. A.; Butler, P. R.; Pilling, M. J.; Baird, J. K. A Solution of the Debye-Smoluchowski Equation for the Rate of Reaction of Ions in Dilute Solution. *J. Chem. Phys.* **1979**, *70*, 4001−4007.
(53) Hunger, J.; Buchner, R.; Kandil, M. E.; May, E. F.; Marsh, K. N.; Hefter, G. Relative Permittivity of Dimethylsulfoxide and N,N-Dimethylformamide at Temperatures from (278 to 328) K and Pressures from (0.1 to 5) MPa. *J. Chem. Eng. Data* **2010**, *55*, 2055−2065.
(54) Craig, M. E.; Crothers, D. M.; Doty, P. Relaxation Kinetics of Dimer Formation by Self Complementary Oligonucleotides. *J. Mol. Biol.* **1971**, *62*, 383−401.
(55) Morrison, L. E.; Stols, L. M. Sensitive Fluorescence-Based Thermodynamic and Kinetic Measurements of DNA Hybridization in Solution. *Biochemistry* **1993**, *32*, 3095−3104.
(56) Gotoh, M. A New Approach to Determine the Effect of Mismatches on Kinetic Parameters in DNA Hybridization Using an Optical Biosensor. *DNA Res.* **1995**, *2*, 285−293.
(57) Kumara, C.; Aikens, C. M.; Dass, A. X-Ray Crystal Structure and Theoretical Analysis of $Au_{25-x}Ag_x(SCH_2CH_2Ph)_{18}$ Alloy. *J. Phys. Chem. Lett.* **2014**, *5*, 461−466.